Chemie der Erde 78 (2018) 479–489

Contents lists available at ScienceDirect

Chemie der Erde

journal homepage: www.elsevier.com/locate/chemer

Aspects of U-Th fractionation in Tertiary limestones and calcretes of Dhofar, southern Oman

Bernhard Pracejus[a,*], Narasimman Sundararajan[a], Salah Al-Khirbash[a], Talal Al-Hosni[a], A. Ebrahimi[a], Shakil Al-Bulushi[a], Ali Al-Lazki[b], Musadem Al-Maashani[c]

[a] Earth Science Department, Sultan Qaboos University, P.O. Box 36, 123 Al-Khoud, Muscat, Oman
[b] Petroleum Development Oman (PDO), Mina Al-Fahal, Muscat, Oman
[c] Ministry of Commerce & Industry, Muscat, Oman

ARTICLE INFO

Handling Editor: Astrid Holzheid

Keywords:
Uranium-thorium fractionation
Limestone
Calcrete
Dhofar
Oman

ABSTRACT

This paper presents findings from a comprehensive geochemical and geophysical re-examination of known radiogenic anomalies in Tertiary limestones and (sub-)recent calcretes of southwestern Dhofar in the Sultanate of Oman. U-Th-enrichments seem to be associated with deep-rooted fault systems that cross-cut C_{org}-rich shales at depths of some 800–1000 m, which generally show elevated gamma-ray levels in southern Oman and act as the initial geochemical trap. Metals and radiogenic elements, such as K (max 1945 ppm), U (max 44 ppm), and Th (max 26 ppm) mobilised from these rocks and emplaced higher up in the faults must have constituted radiogenic lineaments at and near the surface (observed in a different but difficult to access location). However, successive weathering partially obscured such anomalies through further re-mobilisation/-mineralisation processes within the calcretes that also enriched Sr and V. In these carbonates, uranium correlates positively with Sr but not very well with V, while thorium shows moderate positive correlations with Sr and V. Both U and Th are also not present (i.e., below the detection limits of a few ppm) in a second sample group that represents background conditions. Being much more immobile than U, Th remained closer to the original western fault positions of the examined site (outlined by magnetics and VLF-EM during the surveys), while uranium moved down-dip over the plateau and through underlying sub-horizontal strata towards the eastern fault system. Here, supergene Sr-enriched calcite preferentially incorporated U, thus reflecting the observed U-Th fractionation.

1. Introduction and geological setting

In 2012, a project was initiated to re-examine sites in the Dhofar region of southern Oman (Fig. 1) that had previously shown anomalous uranium (U) enrichments in the form of carnotite ($K_2(UO_2)_2(VO_4)_2{\cdot}3H_2O$) in Tertiary micritic (EOzl) and lacustrine (Oaq) limestones (Fig. 2a and b). These fairly uniform rocks cover a fairly large area of some 450 km^2 and are heavily cross-cut by sub-parallel mineralised fault systems with a general NE-SW strike (Quidwai, 1981; Quidwai and Khalifa, 1982; Wynes and Platel, 1992). Some of the veins, particularly those in the southwestern parts of the research area, are concealed by recent to sub-recent calcretes. Where accessible, the veins show U concentrations far above the background values (< 2 ppm) found in the vicinity, which already points to a more focused emplacement of the radiogenic elements. Embedded within the underlying carbonate sequence are the carbonaceous shales of the Andhur Formation (Edm1), which are important for our further interpretation. Not much is known about the actual depth of the Precambrian crystalline basement of the Arabian-Nubian Shield within the research area (here, only few oil exploration drills have intercepted basement rocks and outcrops are scarce), but it probably lies deeper than 2 km (see, for instance, Figure 19.2 in Forbes et al., 2010) and we assume that it is similar to the basement outcropping east of Salalah (some 120 km east of the research area), which is composed of micaceous and occasionally K-feldspar-rich felsic rocks (granite, granodiorite, tonalite), paragneisses, amphibolites, and an ultramafic complex (Mercolli et al., 2006; Allen, 2007; Hersi et al., 2012). In places, these rocks are cross-cut by swarms of macro-crystalline felsic (pegmatitic) and mafic dikes.

Occasionally, the mentioned calcretes also have accumulated uranium (Howari et al., 2016). However, although some large uranium mineralisations in younger carbonate rocks are known (Gabelman and Boyer, 1988), they are still fairly uncommon because most major uranium deposits occur in Precambrian rocks. Between 2012 and 2016, geochemical and geophysical surveys were conducted in the area to

* Corresponding author.
E-mail address: pracejus@squ.edu.om (B. Pracejus).

https://doi.org/10.1016/j.chemer.2018.09.003
Received 25 November 2017; Received in revised form 18 September 2018; Accepted 18 September 2018

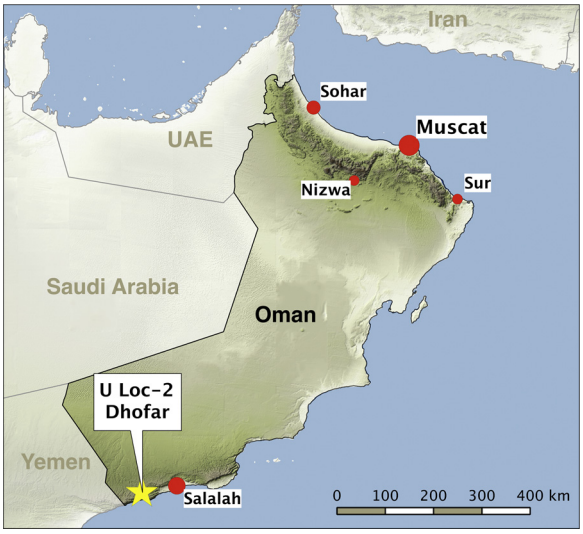

Fig. 1. Overview map of Oman with the research area Loc-2 in Dhofar; site Loc-4 is nearby. The map was produced with SimpleDEMViewer for Mac (version 4.4.9), ASTER GDEM data (product of METI and NASA), QGIS (version 2.0.1-Dufour) under GNU General Public License.

develop exploration concepts for this particular geological setting and to determine the economic potential of the mentioned sites (plus other areas around Oman). During this research it was noted that a number of samples indicated a spatial separation of uranium (U) and thorium (Th), a finding that is presented below.

1.1. Generalised geology of uranium deposits

Uranium is a fairly mobile element with a low crustal abundance of some 2–4 ppm (Evans, 1993). In the reducing atmosphere governing early geological processes on Earth, mainly erosional processes concentrated the high density uranium minerals in placers (without much geochemical redistribution), while successive oxygenation episodes of the atmosphere and associated chemical weathering caused the mobilisation, transport, and redeposition of uranium (Marmont, 1989) in large deposits focussing along unconformities.

Being fairly young in geological terms (Tertiary), the examined anomalies in the limestones of Dhofar (western Oman) vary considerably from most of the large variety of uranium deposits (IAEA, 1988), which is outlined below according to the respective geological settings (not in order of their economic potential; IAEA, 1984, 1985, 1986, 1987, 2009). Various other combinations of classification parameters are also possible, such as uranium source, fluid and rock character, enrichment and mineralisation processes, but were not included here for clarity (Gabelman, 1988):

- **Unconformity-related deposits** occur in the immediate vicinity of major unconformities (i.e., below or above) separating igneous basement and overlying clastic sediments. Metasediments near the boundary are usually faulted and brecciated and are the locus of the main mineralisation.
- **Igneous environments** (intrusive and extrusive) not only include *intrusive rocks* per se, but *vein deposits* (granite-related; fillings of voids, such as cracks, veins, fissures, pore spaces, breccias, and stockworks), *pegmatites containing rare metals* (Sn, Ta, Nb, Li, and REEs), *volcanic- and caldera-related deposits* (forming veins or disseminations in acid to intermediate rocks related to faults and shear zones), and *hematite breccia complex deposits* (associated with a near surface explosive event involving boiling processes).
- In **metamorphic deposits**, the uranium enrichment can directly derive and concentrate from the *metamorphosed rock*, while *metasomatic processes* (e.g., Na metasomatism) lead to a re-distribution of U via leaching, transport, and mineralisation in the form of disseminations within structurally deformed rocks (Precambrian shields).
- With the exception of *phosphorites* (marine and of continental-shelf origin), **sedimentary uranium deposits** show the significance of carbon, producing a reducing environment and adsorbing uranium on *lignite* (coal), organic matter in *black shales* (also carbonaceous pyritic shales) or *sandstone deposits* (medium to coarse-grained continental fluvial or marginal marine sediments; categorised as *roll-front, tabular, basal channel,* and *tectonic/lithologic deposits*). While the geological environment of some Archaean to early Palaeoproterozoic *quartz pebble conglomerate deposits* with detrital uraninite could also be classified as metamorphic environments, they clearly indicate reducing conditions (anoxic atmosphere, prevalence of hydrocarbons at least during overprinting; (Pracejus, 2015, pp. 866–867). Last, but not least, hydrocarbons occasionally also enrich uranium.
- **Weathering environments** (including **karst) and soils** are grouped into *limestone and paleokarst deposits* (intra-formational folds and fractures acted as geochemical traps), *collapse breccia pipe deposits* (vertical circular collapse structures containing coarse breccias with large open pore space for fluid migration and mineralisation), and geologically young *surficial deposits* (Tertiary to recent) in sediments or soils. Calcretes contain the largest deposits of this type, on which the present paper will concentrate.

1.2. Uranium fractionation mechanisms

Fractionation processes between uranium and thorium can broadly be categorised in the following scheme:

- ***Igneous and metamorphic processes*** govern the incorporation into specific igneous or metamorphic minerals, which leads to a separation of the two elements (Condomines et al., 1981; Elliott, 1997; Krishnaswami et al., 1984; Landwehr et al., 2001; LaTourrette et al., 1993; Nishimura, 1970; Oversby and Gast, 1968; Spiegelman and Elliott, 1993). Mechanisms controlling the fractionation are oxidation processes during fractional crystallisation (Ragland et al., 1967) and magma mixing from materials such as depleted and enriched mantle (Newman et al., 1984).
- ***Water-related mechanisms*** affect the re-mobilisation, transport, and re-mineralisation of uranium and thorium, with the former being much more mobile than the latter (Dabous et al., 2002). This differing behaviour is reflected in the formation of a large variety of uranium chloride, carbonate, phosphate, and sulfate complexes in aqueous solutions, while thorium hardly establishes comparable compounds (Langmuir, 1978; Keppler and Wyllie, 1990). Newly forming minerals, such as carbonates in weathering environments, can therefore be expected to reflect the prevailing U-Th enrichments in the respective surface-/groundwaters. Similarly, biomass such as plant matter or coal will accumulate significantly higher concentrations of uranium, because of the incorporation of soluble compounds from groundwaters, which is easier than collecting substances derived from rocks and minerals (Vargas et al., 1997). Within volatile-rich melt systems, both elements form fluoride complexes in the fluids, particularly increasing the mobility of uranium (Keppler and Wyllie, 1990) and leading to a stronger redistribution of U when compared with Th (Condomines et al., 1987).
- ***Adsorption processes*** occur on various minerals, such as clays (Min et al., 2005) and organic matter (humic compounds; Ahmed et al., 2014). The amount of adsorbed uranium and thorium is probably again controlled by their respective response to complexation and related mobility of the two elements. An adsorption of the uranyl ion is maximal in the pH range between 5–8.5 (Langmuir, 1978).
- ***Microbial metabolic processes*** can be expected to also influence the

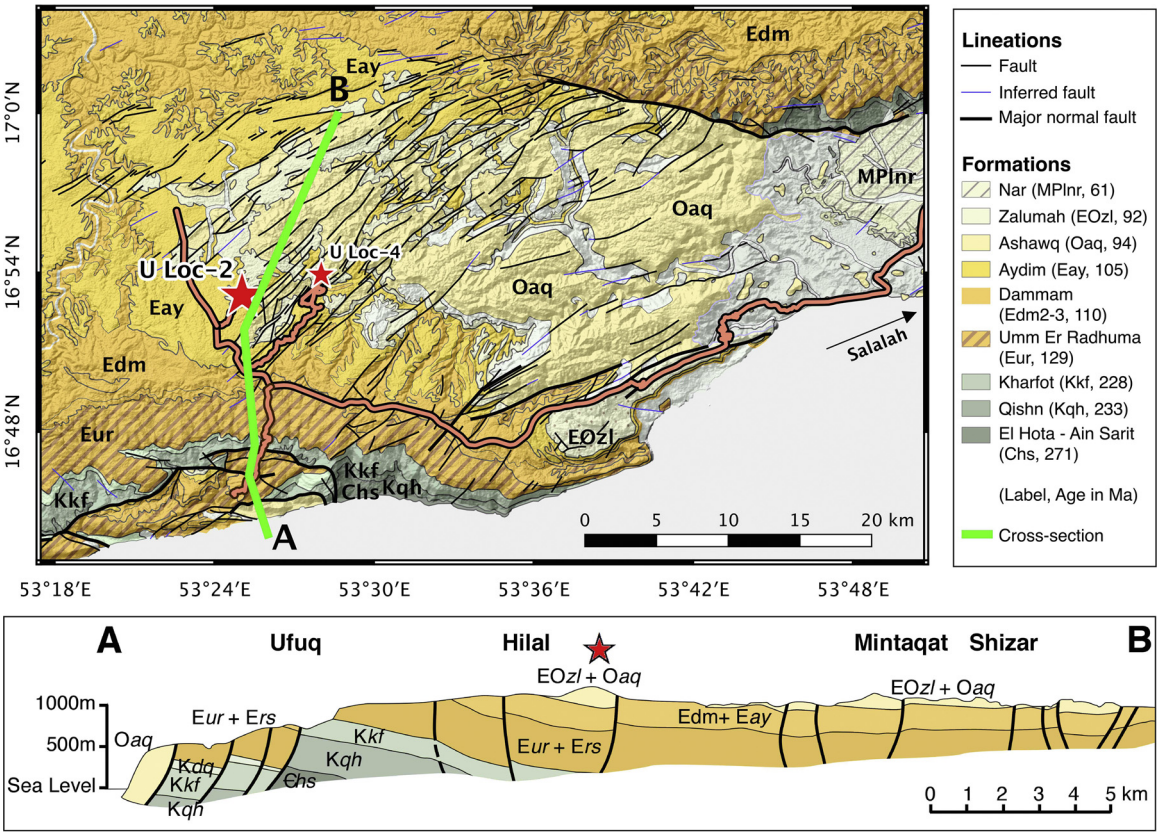

Fig. 2. a) Overview of the southwestern Dhofar region west of Salalah showing the tectonic setting of the exploration targets U Loc-2 and U Loc-4; b) geological profile (see green line from A to B) close to the site U Loc-2; map and profile are modified after the geological map of Oman W of Salalah (Béchennec et al., 1993). The map was produced with SimpleDEMViewer for Mac (version 4.4.9), ASTER GDEM data (product of METI and NASA), QGIS (version 2.0.1-Dufour) under GNU General Public License. (For interpretation of the references to colour in this figure legend, the reader is referred to the web version of this article.)

fractionation of U and Th. According to Basu et al. (2014), bacterial reduction of U(VI)-containing minerals results in isotopic fractionations that partition heavier isotopes into the solid U(IV)-minerals (Basu et al., 2014). This is likely to also have a bearing on separation processes affecting uranium and thorium.

1.3. Uranium in Oman – previous work

The history of uranium exploration in Oman dates back to 1979, with the first discovery of carnotite ($K_2(UO_2)_2(VO_4)_2{\cdot}3H_2O$; Quidwai, 1981; Quidwai and Khalifa, 1982; Wynes and Platel, 1992). Many of these findings cluster near the locations shown in Fig. 2a, concentrating in the strongly faulted block in the center of the map. Fractures coated with carnotite were, for instance, identified in a chalky limestone layer in the Mughsayl formation. Carnotite was also reported from the Thumrait area in Wadi Dahaban, disseminated in a 2 m thick limestone layer of the Rus Formation, and coating joints and fractures in the same formation at Wadi Gharbatan. According to BRGM (1984), the described anomalies occur exclusively within a stratiform setting and are associated with two mineralised host horizons within the Zalumah and Ashawq formations of the Dhofar Group, corresponding to episodes of continental influence within littoral marine deposits. The radiometric anomalies correlate well with carnotite occurrences in paleo-channels of sandstones, carbonaceous materials, and calcretes.

Although this paper does not focus on the geology and structural setting of the region, it is necessary to briefly mention here that in contrast to the mentioned previous work, which interpreted the two mineralised horizons as purely stratiform, we see these anomalies as being strongly fault-controlled (Béchennec et al., 1993, compare Fig. 2). The limestones of the region generally show uranium values below 2–3 ppm and a 10- to 20-fold increase in radiogenic elements focused in particular locations must entail a source, a conduit, a mobilisation and transport mechanism, and a precipitation process for uranium and thorium.

Radiogenically much more active rocks (C_{org}-rich shales) appear in the Tertiary Andhur formation at depths between 800 and 1000 m (Forbes et al., 2010, Table 1) and could be interpreted as protores for the enrichments. When examining the more or less intensely mineralised sites in detail, it is evident that they all focus on and around faults, of which some do not extend to the surface because of their recent to sub-recent calcrete cover (Sundararajan et al., 2017, 2016; Sundararajan et al., 2015a, 2013, 2014, 2015b). These faults must have acted as conduits for the observed U-Th enrichments, connecting protores with the current sub-surface to surface loci of the mineralisations. There, a change in lithology and physicochemical conditions led to the fixation of the radiogenic elements, while subsequent weathering

Table 1
Overview of the geological rock units of the research area.

Label[a]	Formation	Age (ma)	Stratigraphic Unit	Description
Qcx-z		24	Quaternary	slope colluvium
EOzl	Zalumah	92	Tertiary	micritic limestones
Oaq	Ashawq	94	Tertiary	lacustrine limestones
Eay	Aydim	105	Tertiary	bioclastic limestones
Edm2-3	Dammam	110	Tertiary	bioclastic limestones
Edm1	Andhur	113	Tertiary	shale and intercalated limestones
Ers	Rus	120	Tertiary	chalky dolomitic limestone & marl

[a] Geological formation.

causes further redistribution and fractionation.

2. Methods

2.1. Field work and materials

Field work in southern Dhofar is often hampered by very difficult and steep terrain. Nevertheless, in situ geochemical analyses with a portable XRF and radiometric profiling with a gamma-ray spectrometer proceeded and provided the presented data (supported by further measurements in the lab). The sub-horizontal plateau of U Loc-2, however, was more accessible for geophysical traverses, because it only dips slightly to the northeast by some 40 m over a distance of 1 km; the research area is approximately 300 m wide. The topographical highs focus in the southern half of the area and lead to a drainage pattern oriented towards the northeast. Eleven parallel profiles up to 300 m long and 100 m apart with a measurement interval of 10 m were acquired on the U-loc 2 plateau. The profiles were laid out perpendicular to the general NE-SW strike of the fault systems in the region. While no fault is visible on the plateau (sealed by recent to sub-recent calcrete?), several sub-surface fault lines were detected during the associated magnetics and VLF surveys. These faults are shown in context with U and Th distributions. A few relatively short profiles were also obtained from a physically challenging steep wadi incision (U-loc 4); the gathered data from this location will only be used in the geochemistry section.

Some 170 samples were analysed by X-ray Fluorescence (XRF) in samples collected from the slopes below the plateau of U Loc-2 (where the geophysical profiles were obtained). Here, various rock units were accessible, in contrast to the geologically very homogeneous plateau. The slopes also encompass the previously known U-loc 2 anomaly, according to which the survey area was framed (Quidwai, 1981; Quidwai and Khalifa, 1982; Wynes and Platel, 1992, Fig. 2). A few additional samples were measured in U-loc 4.

The examined materials mostly consist of fairly massive limestones with small amounts of clays and iron oxyhydroxides, which stain the rocks with creme to light orange-brown shades. Although geochemically very similar to the surrounding limestones, the materials of the small U Loc-2 anomaly are very friable and dust-like. In contrast, the U Loc-4 site (see Fig. 2) was contained in a mineralised sub-vertical fault consisting of massive carbonate.

2.2. Geophysics – gamma-ray spectrometry

Although a number of different geophysical techniques were used in the investigations, such as gravity, magnetics, and VLF-EM, the primary tool for outlining the encountered anomalies was gamma-ray spectrometry (Gamma Ray Spectrometer BGO Super RS-230), which measures the radiation of potassium (K), uranium (U), and thorium (Th) as the three most abundant radiogenic elements.

2.3. Geochemistry – X-ray fluorescence (XRF)

A Niton XL3t 950 handheld XRF Analyzer (Thermo Scientific) was used in the field to directly examine anomalies pointed out by a gamma-ray spectrometer (see below). The device is equipped with an SDD GOLDD + Detector and an Ag-anode X-ray tube; it has an excitation voltage of 50 kV (200 mA, 2 W). Emitted X-rays excite a secondary spectrum from the sample material, which is then detected and analysed by the instrument, providing compositional data for some 55 elements. The instrument uses an auto-calibration at each start-up. Such portable devices are widely used in geochemical exploration.

2.4. Thermodynamic modelling

The thermodynamic stability for dissolved and mineralised uranium and thorium compounds were calculated and plotted with the “Act2” module from “The Geochemist's Workbench” (Bethke, 2008, version 8.0). Dissolved carbonate concentration was assumed to be close to that of normal surface waters of 10^{-3} Mol/l (Brookins, 1983). While calcium and potassium levels were modelled at relatively high concentrations (limestones and evaporites contribute to the dissolved species), uranium, thorium, and vanadium were set to low concentrations to mimic their possible release form existing mineralisations within the weathering environment of a desert.

3. Results

The plateau on which the geophysical survey was conducted presents itself as a sub-horizontal area with strong incisions from adjacent wadis. The relatively steep slopes below the plateau are often covered with recent to sub-recent slope colluvium, small cliffs of a few meters hight provide outcrops of the rocks immediately underlying the surface of the plateau; geochemical sample analyses from here are discussed in the geochemical section.

3.1. Radiometric survey (U loc-2)

The measurements of the gamma-ray spectrometer show that potassium is by far the most concentrated radiogenic element in all sites (~ 800 times more than uranium and thorium together), while uranium shows values roughly 3 times above thorium. The distribution among these elements is fairly homogenous, because all of the plateau sites are located within the same rock unit. However, some analyses are completely lacking either thorium or potassium (Fig. 3); comparable observations relating to U and Th were made in the geochemical survey.

Fig. 4 depicts the results of the radiometric survey, first showing the location and orientation of the work area on the geological map (red plateau outline in Fig. 4a) and then depicting uranium and thorium anomalies on the plateau (Fig. 4b, c). From these images, it is evident that U concentrates in the northeastern parts of the plateau, although the most prominent anomaly in the SW (but below the plateau) with up to 44 ppm U near the red star marking (gamma-ray and XRF analyses) does not reflected much of this enrichment (Fig. 4b). Thorium, on the other hand, seems to be much more widespread and evenly distributed, aligning with the depicted faults (black lines) in a NE-SW strike fashion, sometimes appearing in sites where U is enriched, in other cases where U is depleted (Fig. 4c).

The two elements, thus, seemingly do not share much of coinciding

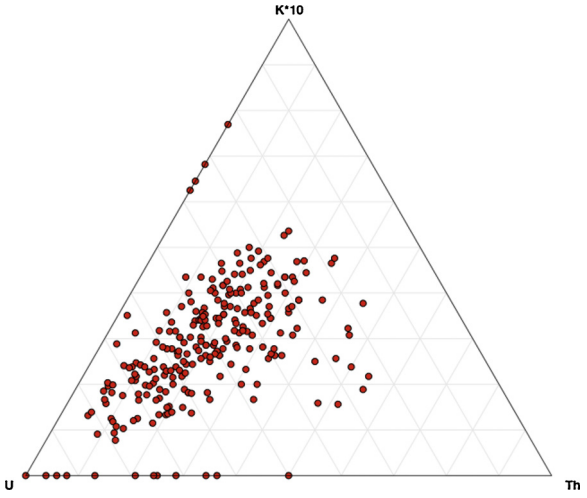

Fig. 3. Ternary diagram illustrating the radiometric data distribution (gamma-ray spectrometer) on the plateau; percent values were used for K (multiplied by 10), while U and Th were directly taken as ppm values.

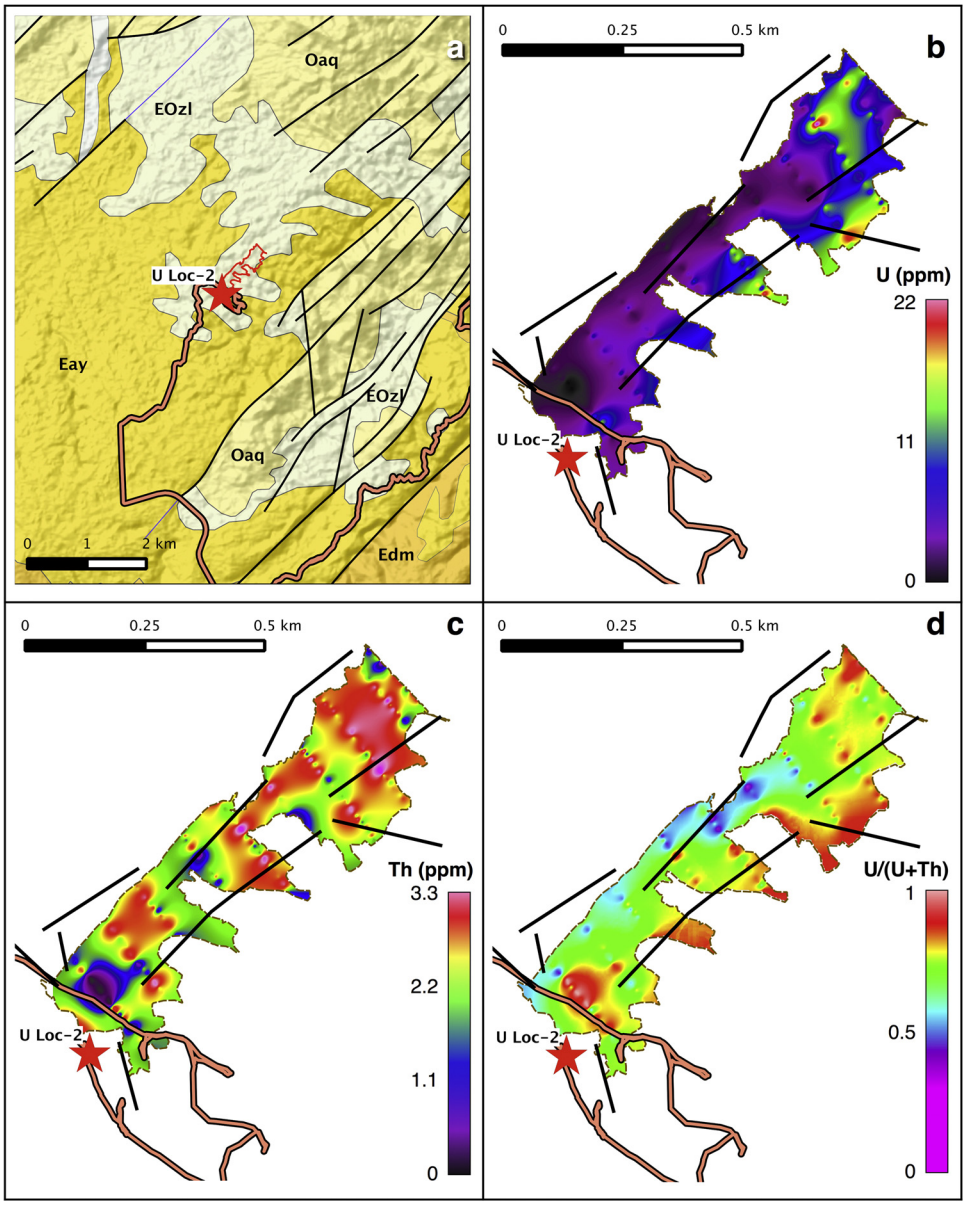

Fig. 4. a) Geological map and location of the U Loc-2 site; the red line shows the outline of the investigated plateau (enlarged in Fig. 4b-d), while the red star indicates the locations shown in Fig. 2; major sub-surface faults mapped out geophysically (magnetics and VLF) are shown as black lines); b) Distribution of radiogenic U (ppm) on the plateau of U Loc-2; c) Distribution of radiogenic Th (ppm); d) Distribution of U-Th Ratio (U/(U + Th)) values over the plateau. Used programs and data sources were: SimpleDEMViewer for Mac (version 4.4.9), ASTER GDEM data (product of METI and NASA), QGIS (version 2.0.1-Dufour) under GNU General Public License, and Béchennec et al. (1993). (For interpretation of the references to colour in this figure legend, the reader is referred to the web version of this article.)

patterns. However, when the ratio between U and Th is plotted (U/(U + Th)); values vary between 0 for Th-rich and U-poor sites and 1 for U-rich and Th-poor sites), a clearer picture emerges (Fig. 4d). Along the southeastern edge of the plateau fault system, uranium seems to be enriched (orange and red) and has separated from thorium (marked by blue and purple) which, in turn, positions itself more closely with the northwesterly trending fault system.

3.2. Geochemical relationships

Although more than 50 different elements were analysed by XRF (Al-Balushi, 2015), not many clear relationships with uranium and thorium are apparent (Fig. 5a–f); occasionally, diffuse negative regressions exist (e.g., Ca, Nb). Common positive inter-element correlations include Si, Al, Fe, Ti, and Zr, which can all be attributed to the low amount of clay minerals and/or sheet silicates of the limestone (Fig. 5a). Outstanding in the entire set of analysed elements, however, are strontium (Sr) and vanadium (V), which depict sample patterns that suggest the presence of two distinctly different materials/minerals (Fig. 5b):

- Variable Sr concentrations (0–1.4%) show low V levels (< 200 ppm),
- High V (~1500–3000 ppm) correlate with low Sr (most < 0.1%).

This clustering also corresponds well with U and Th and is a good indicator for possible mineralogical affinities. When plotted against uranium and thorium, strontium depicts one well-developed positive regression pattern and, in a second group, variable amounts of strontium without U or Th (Fig. 5c and e; Zr versus U or Th produces very similar diagrams). Vanadium, on the other hand, produces one cluster at high V values with relatively low U and Th, while another group hardly shows V but is quite variable in uranium and thorium (Fig. 5d and f).

The de-coupling of uranium and thorium is prominently displayed in a ternary plot for Th and U versus Sr that integrates both examined locations (Fig. 6a):

- Characteristic sample groups from both sites either contain no Th or U, while
- U Loc-2 shows a third intermittent group of mixed samples that become enriched in U and Sr and

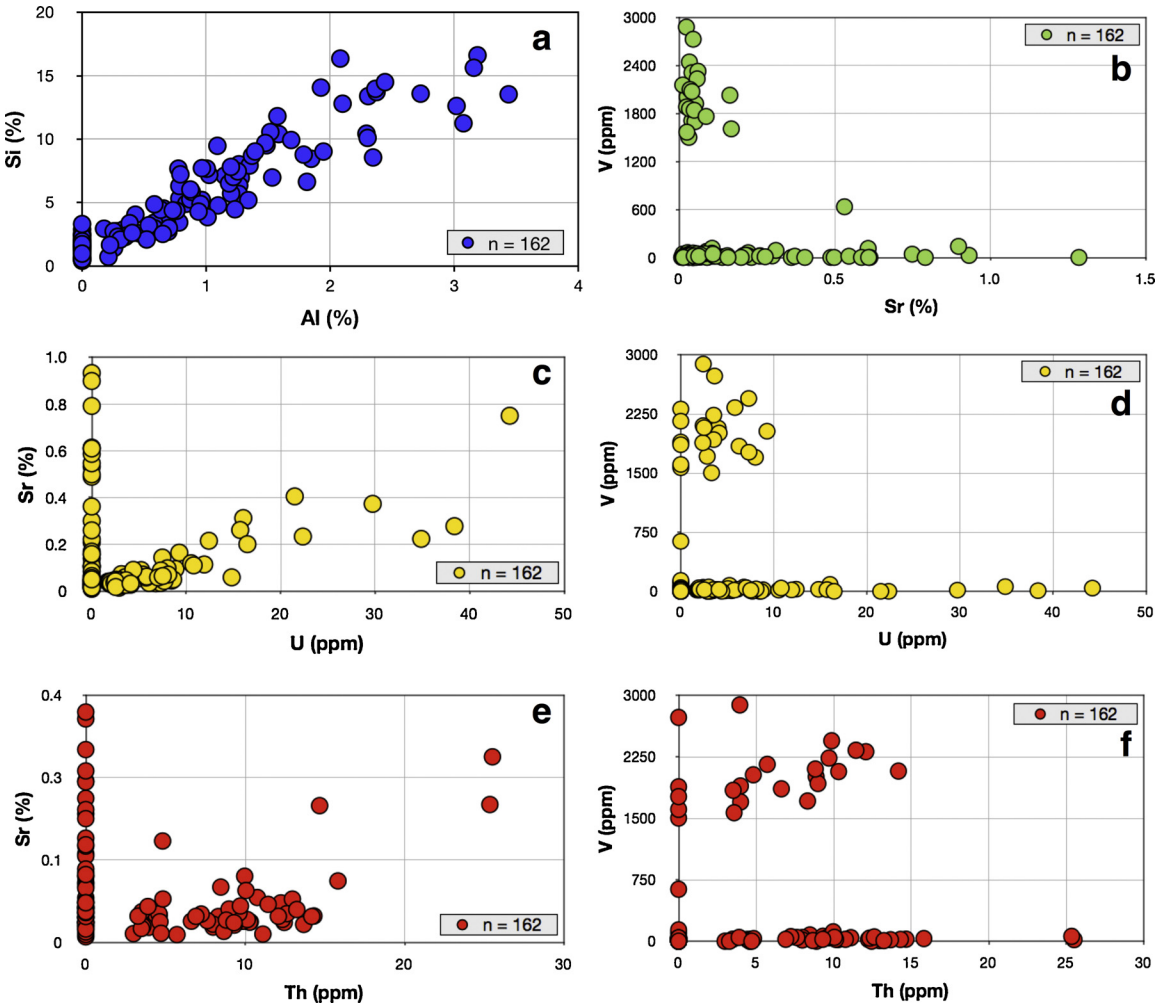

Fig. 5. Regression patterns of major, minor, and trace elements from U Loc-2: a) Si versus Al, depicting a close relationship between the two elements relating to subordinate clay components in the limestone; distinctive separation patterns for b) Sr/V, c) U/Sr, d) U/V, e) Th/Sr, and f) Th/V.

- U Loc-4 has an additional pattern of increasing U in parallel to decreasing Sr values.

The differences between both locations are also apparent in distinctive groups of the ternary diagram U versus Sr and V (Fig. 6b). Here, uranium clearly shows higher uranium concentrations in U Loc-4 when compared with U Loc-2, although many samples again illustrate the absence of uranium, particularly in U Loc-2.

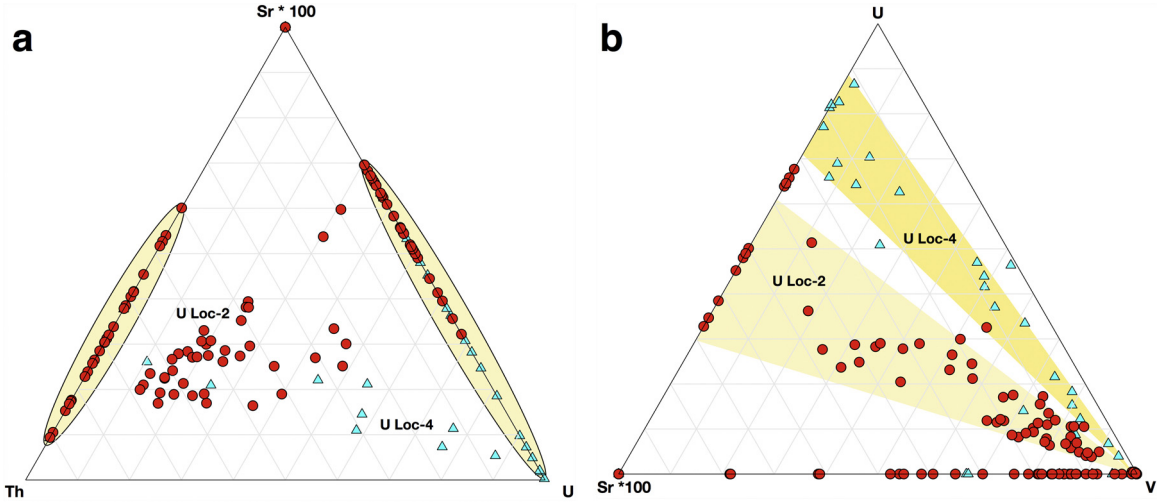

Fig. 6. Ternary diagrams of a) strontium against thorium and uranium and b) uranium versus strontium and vanadium; both diagrams depict XRF data from U Loc-2 and U Loc-4; n ~ 200.

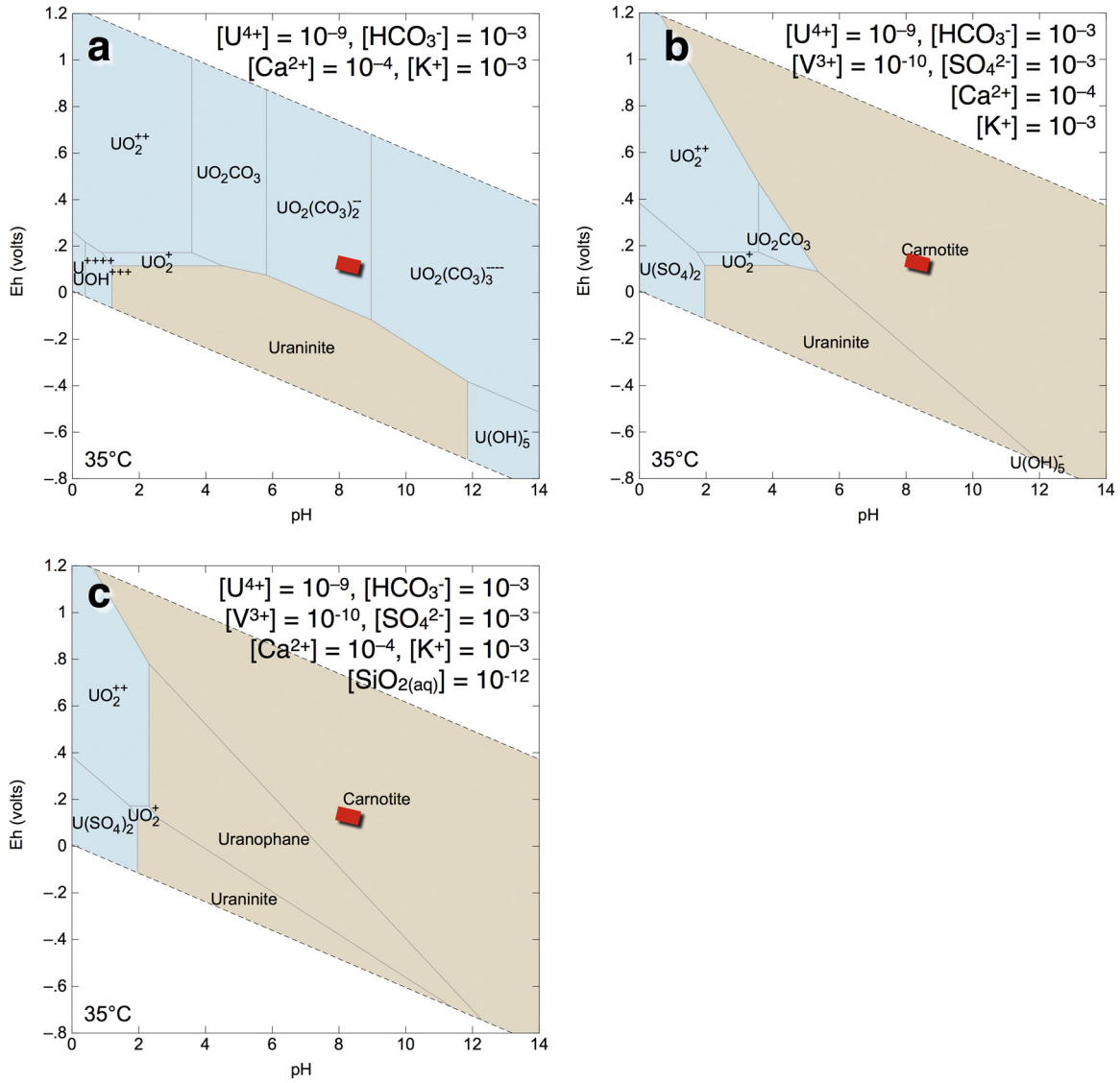

Fig. 7. Thermodynamic stability fields for uranium species: a) dissolved carbonate and hydroxides species dominate, b) low vanadium concentration and K > Ca produces a large field for carnotite, while an addition of sulfur to the system only results in a small field for dissolved U sulfate under extreme acid and reducing conditions, c) additional low amounts of dissolved silicate replaces parts of the carnotite, uraninite, and dissolved U species stability fields; the red bar indicates pH/Eh conditions of surface waters from the field area (see below); after Bethke (2008). (For interpretation of the references to colour in this figure legend, the reader is referred to the web version of this article.)

3.3. Thermodynamic stability of U and Th compounds in aqueous environments

The thermodynamic modelling of uranium and thorium stability fields (Figs. 7a–c and 8 a–c, respectively) clearly explains the strong mobility differences of both elements in natural environments (Bethke, 2008). The modelling temperature was set to a slightly higher value than measured in the cold season to suit an environment that is easily attained during the hot summer months in Oman. Although not apparent in any of the displayed models, comparatively high strontium (Sr^{2+}) concentrations were also part of the modelling of both elements (our analyses illustrate important affinities) but show no effect on any stability field; neither do calcium and potassium in the thorium modelling. No further components other than ambient levels of dissolved carbon are included in the initial model to mimic simple surface water conditions in the field area (Figs. 7a and 8 a).

While a large variety of dissolved carbonate and hydroxides species are omnipresent together with uraninite (UO_2; Fig. 7a), thorium only displays a very large field for thorianite (ThO_2) and a minor field for Th^{4+} under acidic conditions, cross-cutting redox boundaries (Fig. 8a). Carbonates do not play a role for thorium and thorianite is the dominating and very stable mineral (Valsami-Jones and Ragnarsdóttir, 1997).

Introducing low vanadium concentrations and K > Ca into both systems produces a large stability field for carnotite ($K_2(UO_2)_2(VO_4)_2{\cdot}3H_2O$; Fig. 7b), while there is no change in the thorium speciation (Fig. 8b). If the K-Ca ratio is reversed (K ≤ Ca), carnotite disappears and is replaced by an almost identical stability field of tyuyamunite ($Ca(UO_2)_2V_2O_8{\cdot}5\text{-}8H_2O$; not shown), which also covers part of the uraninite field. Sulfate addition, on the other hand, causes the formation of an aqueous sulfate species (not sulfide!), even in a fairly reducing and acidic environment in the case of uranium (Fig. 7b) and a relatively small field of thorium disulfide (ThS_2; Fig. 8b).

Uranium speciation is also altered by the presence of dissolved silica (Fig. 7c). Even very low silica concentrations force the formation of uranophane ($Ca(UO_2)_2SiO_3(OH)_2{\cdot}5(H_2O)$) which with increasing silica levels covers large portions of the pH/Eh space. In strong contrast, thorium is not affected and shows no tendency to form a mineral with

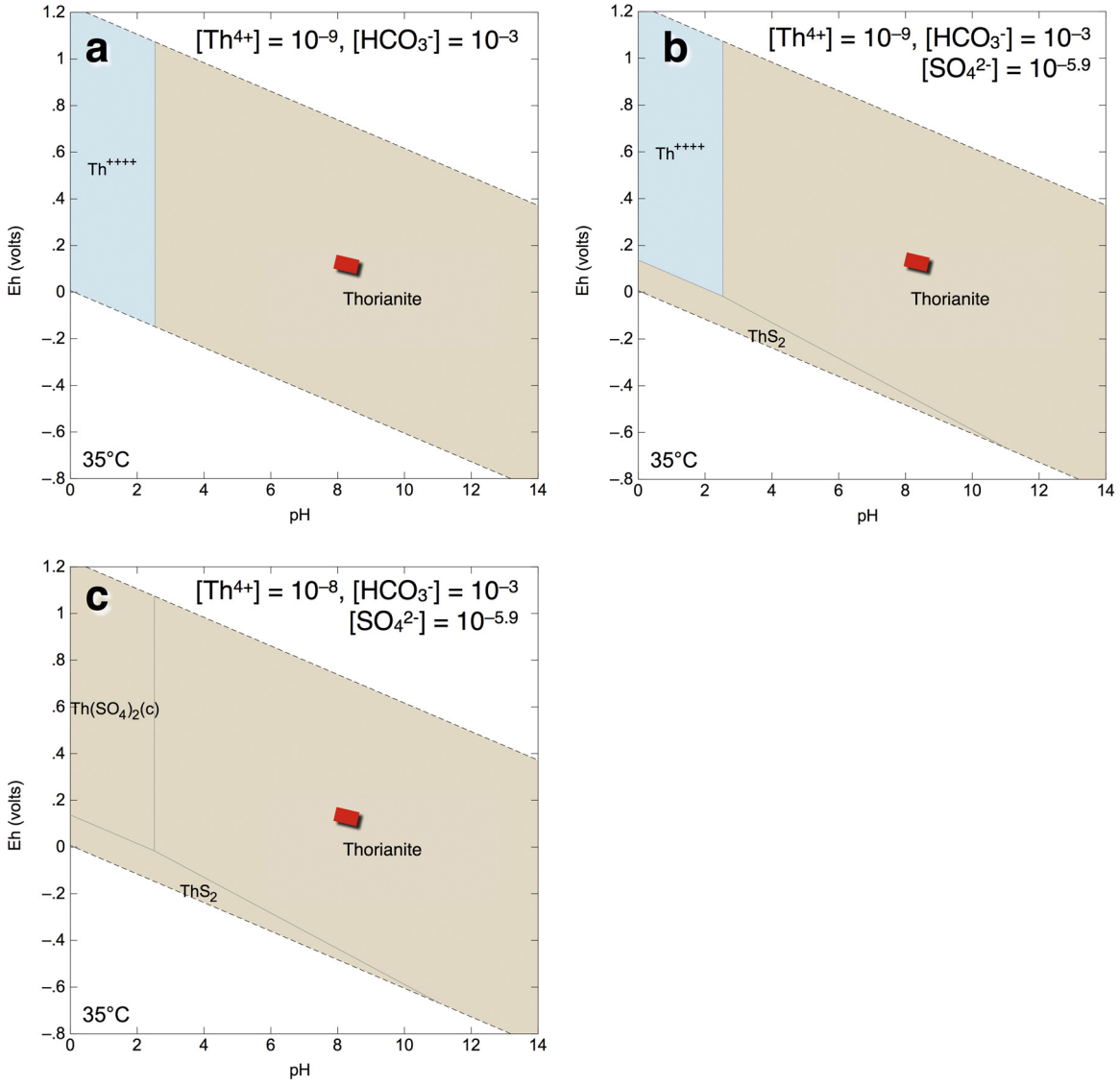

Fig. 8. Thermodynamic stability fields for thorium species: a) dissolved carbonate does not affect Th speciation, while much of the pH/Eh space is covered by thorianite b) an addition of sulfur to the system only opens a small field of Th sulfide (not known in nature) under strongly reducing conditions; c) a slight Th increase with all other conditions unchanged replaces the dissolved Th^{4+} field with thorium sulfate; the red bar indicates pH/Eh conditions of surface waters from the field area (see below); after Bethke (2008). (For interpretation of the references to colour in this figure legend, the reader is referred to the web version of this article.)

silica. However, if thorium abundance builds up (compare Fig. 8b and c: changed from 10^{-9} to 10^{-8} Mol/l), the Th^{4+} field gets replaced by the solid thorium disulfate ($Th(SO_4)_2$; not found in nature; Fig. 8c).

The red bar shown in Figs. 7 and 8 indicates pH/Eh conditions of surface waters measured in the field area during one of the surveys (Table 2). In the case of a carbonated environment (Fig. 7a), uranium would be mobile, while K^+ and V^{3+} put the system into the carnotite stability field (Fig. 7b and c). Thorium, on the other hand, cannot be transported in any of the discussed scenarios and would precipitate immediately as thorianite, if it had been liberated during the breakdown of a Th-containing mineral (Fig. 8a–c).

Table 2
Hydrochemical parameters of two small ponds in a wadi next to the U-loc 4 position.

Sample	pH	Eh (mV)	T (°C)
Dh U4/1	8.15	130	27.7
Dh U4/2	7.50	153	30.8

4. Discussion

In this study, we focus on the relatively young sub-horizontal layers of Tertiary micritic (EOzl) and lacustrine (Oaq) limestones including calcretes (surficial deposits) that are cross-cut by mineralised fractures (veins) and the accompanying radiogenic anomalies. An understanding of these fault systems is crucial to the identification of possible distribution and precipitation mechanisms for the uranium (and Th) mineralisations. Since the limestones/calcretes of the region are principally void of radiogenic elements, it is the faults that present the conduit for U-Th-V-Sr-Ca-enriched fluids deriving their compositional load from underlying C_{org}-rich shale strata (compare (Khoury et al., 2014). The possible means of geochemical transport and collection in the "final" traps for U and Th are discussed below, together with feasible fractionation processes.

At pH values above about 7 (the local surface waters fulfill this requirement with pH values between 7.5 and 8.15; Table 2), the uranyl ion forms strong aqueous complexes with carbonate (Grenthe et al., 1992; Langmuir, 1997), inhibiting sorption or fast precipitation of U (VI), although calcrete environments with complete evaporation of the

mineralised fluids would force these components out of solution. Nevertheless, carbonate and bi-carbonate are common anions in groundwaters and probably also dominate the species within the limestones and calcretes of Dhofar (Langmuir, 1997). At slightly more acidic conditions (below pH 7), cations like $(UO_2)_3(OH)_5^+$ prevail and can be adsorbed by humic compounds (Noller et al., 1997). Plants, in general, can play an important role in the fractionation of natural radionuclides through their water uptake, in which certain dissolved compounds dominate according to their respective mobility (Blancoa et al., 2005). This would mean that the most mobile radiogenic element uranium could be efficiently sequestered into the plant where it would concentrate, while the much less mobile thorium may not even reach the root systems. Biology-induced redox and pH changes (such as those from photosynthesis or sulfate reduction) may then induce carbonation and successive mineralisation. However, the plant cover of the region at present is minimal (Warren and Haack, 2001), paleoclimatic information for the time of U/Th mineralisation is not available, and a discussion about this topic remains superfluous, because at present nothing is known about the actual timing of the U/Th transport and fixation as well as a possible extension of these mechanisms into the presence.

Microbial activities, such as those found in soils and surface waters and associated with the biomineralisation of metals (e.g., Fe and Mn in microbial mats; Akhtar et al., 2007; Bender and Phillips, 2004) that could accumulate U, Th, and V, are surely very limited near and at the surface of the Dhofarian limestones because of the current arid climate. The mineralised products of manganese- and iron-oxidising microbes are also insignificant in abundance (the only loose MnO_2 sample of possible hydrothermal origin found in the field - relatively rich in Pb - had negligible U and Th concentrations), otherwise these minerals would have participated in the fractionation of the radiogenic materials to a larger degree, for which there is no indication (Bargar et al., 2009; Benzerara et al., 2011; Francis and Tebo, 2002; Hohmann et al., 2010; Spiro et al., 2010; Tebo et al., 2005).

As mentioned above, the observed pH values appear within a mildly alkaline range, which shifts strontium (and uranium) into environmental conditions roughly equivalent to seawater, where both elements could be taken up by carbonate. Thompson and Livingston (1970) reported this for aragonite precipitation in modern corals (see also Abu-Hilal, 1994; Russel et al., 1994). A similar effect seems to present in those calcium carbonate samples in which uranium and, to a lesser degree, thorium concentrations correlate excellently with Sr (Fig. 5c and d). These are the limestones/calcretes that carry elevated U levels (up to 44 ppm) with calcite being the main host, while there are also many samples with U levels below detection limit ($\leq$ 1–2 ppm); these reflect the background of the region and are typical for U-deficient C_{org}-poor light-coloured limestones/carbonates. We ascribe these findings to diagenetic processes and/or calcrete development in which Sr and U co-precipitate (IAEA, 1984). How far carbonate precipitation induced by Sr resistant bacteria (Achal et al., 2012) or biosorption of Sr during carbonate formation may have assisted in the observed U enrichment in the developing calcretes is not clear, but such processes should not be ruled out (Pan et al., 2009).

In strong contrast to Ca and Sr, U and V are both susceptible to redox variations and also correlate well with each other. This suggests a common precipitation process, which has indeed been documented with the description of carnotite $(K_2(UO_2)_2(VO_4)_2{\cdot}3H_2O)$ in several locations of Dhofar (Quidwai, 1981; Quidwai and Khalifa, 1982; Wynes and Platel, 1992). Carnotite and its Ca and Na equivalents (tyuyamunite and strelkinite, respectively) seem to be common mineral phases in many calcretes around the world (Khoury et al., 2014), although a lack of sodium and a dominance of K over Ca in the Dhofarian waters, from which the described carnotite precipitated, have apparently promoted the latter formation. Thorium does not enter carbonate lattices in large quantities, although it is produced from the decay of U isotopes, and it would thus be separated from uranium (White, 2015).

Silicate minerals acting as ion exchangers, such as zeolites (Misaelides et al., 1995) or adsorbers like muscovite (Schmidt et al., 2012) and causing a concentration of radiogenic elements do not occur in the Dhofar limestones and play no role in any of the local U-Th sequestration processes. There is also very little evidence of dissolved silica having moved through the limestones and calcretes with local pore-/ground- or surface-waters; one exception is reflected in a local small-scale chert nodule formation (not in direct association with the examined anomalies or elevated radiation levels). Minute concentrations of $H_4SiO_{4(aq)}/H_3SiO_4^-/H_2SiO_4^{2-}$ at slightly more reducing conditions than encountered in the field would also cause a prevalence of uranophane (compare Fig. 7c; at larger levels it quickly replaces much of the carnotite stability field). However, uranophane has never been documented from the area under investigation and this absence together with the lack of the mentioned silicate minerals supports our interpretation that silicates don not participate in any of the fractionation processes.

The same consideration applies to phosphorous. Although phosphates may be important in the accumulation of uranium elsewhere (Macaskie et al., 1992; Beazley et al., 2007; Jroundi et al., 2007; Miot et al., 2009) – there is only a weak positive correlation between U and P in our samples and many values are below the detection limit for P – a formation of apatite, Fe or Pb phosphates is at least insignificant and cannot be proven so far (Templeton et al., 2001). The plant cover of the region, which could also release accumulated phosphorous into the aqueous system through microbial degradation of plant matter (Goulhen et al., 2006), is quite poor and would not deliver appreciable amounts of phosphate for such mineralisation.

5. Conclusions

Our field observations do not indicate any larger-scale hydrothermal activity that might have affected the limestones: Only one loose Mn oxide sample with increased Pb levels but quite low levels of other base metals was found during all field campaigns in Dhofar; sulfur concentrations are also insignificant. Thus, radiogenic sources in felsic bedrocks occurring at much greater depths than the Andhur shales are unlikely to have supplied the fault systems with the encountered U and Th. Further elements that could have leached from felsic and metamorphic rocks, such as Si or P, also do not appear in the mineralisations to form uranium silicates or phosphates and have, therefore, not participated in the fractionation of U and Th. The isolated outcrops of granites and metamorphic rocks in the region (Mirbat east of Salalah) also substantiate this view with radiogenic levels typical for the background of such rocks (often, they are even below the expected concentrations).

In contrast to these rocks, C_{org}-rich shale generally acts as geochemical trap for radiogenic elements and trace metals (e.g., V). These sedimentary rocks should be considered protores for secondary re-mineralisation elsewhere (Goldberg and Humayun, 2016; Leventhal, 1991; Ohkouchi et al., 2015; Zhang et al., 2015), particularly in view of the encountered vanadium and its strong positive correlation with U and Th.

Therefore, the available evidence and theoretical considerations can be summarised in the following sequence of events that affected the initial low-level U-Th anomalies and led to the fractionation of the radiogenic elements (Fig. 9; successive numbers in the following points reflect the respective steps of the schematic diagram):

- A pre-enrichment with radiogenic elements as well as trace metals, such as vanadium, occurred in C_{org}-rich shales (1).
- Deep-rooted faulting in the western parts of the plateau, which did not cross-cut the present-day top of the current limestone/calcrete sequence (thus younger than the faulted units) but intersected the shales at a depth of some 800–1000 m, opened conduits along which ground- and surface-waters could migrate (2).

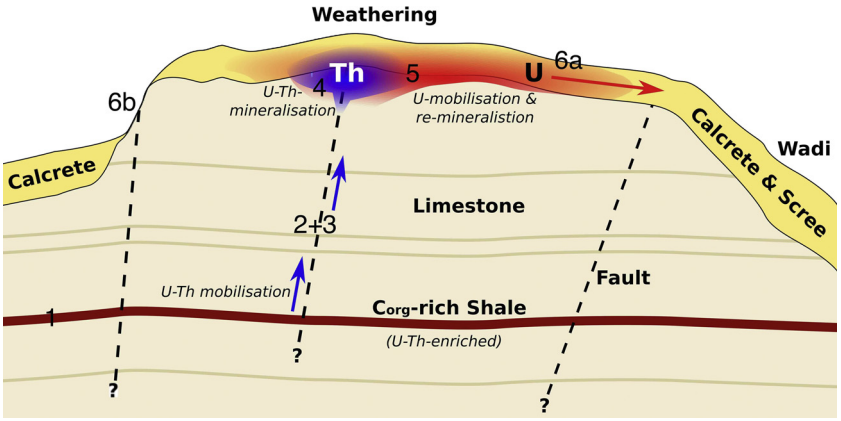

Fig. 9. Simplified overview of the mobilisation, redistribution, and separation of the radiogenic elements in the research area; numbers in the diagram relate to the respective numbers contained in the text.

- These fluids changed the geochemical environment of the encountered shales to more oxidising, thus liberating and transporting radiogenic elements (3).
- Successive near-surface carbonate mineralisation (including Sr) associated with a co-precipitation of U-vanadate within the upper portions of the western faults (observed in U-loc 4; however, no evidence for vanadate) led to the emplacement of a first radioanomaly; such mineralistions are not strata-bound (4).
- Surface weathering then mobilised and dislocated carbonates (and possibly vanadates) from upper limestone portions and fault fillings (plus their associated element content). The more mobile uranium was subsequently transported down-dip over the plateau towards the eastern faults and into the underlying strata and the neighbouring wadi (see Fig. 4a–d), while Th remained closer to its original fault-near position because of its immobility. This U-dominated dislocation caused a lateral separation of the two elements (5).
- Newly forming calcrete now covers the possible fault outcrops in many places (6a; except where erosion has removed it as, for instance, in U-loc 4; 6b) then preferentially took up uranium (together with strontium), while vanadium also mineralised as the second U-carrier (carnotite). The remaining low Th levels of the surface waters were not incorporated into any of the precipitates and were ultimately washed out, leading to a clearly observable fractionation.

Conflicts of interest

None.

Acknowledgements

The authors wish to express their appreciation for the financial contribution received from a strategic grant to Sultan Qaboos University (His Majesty's Grant - SR/SCI/ETHS/12/02), which funded the uranium research campaign in Oman from 2012 to 2017. We acknowledge the field support from our students (in alphabetical order): Zaher Hamed Said Al-Aamri, Mohammed Salim Mohammed Al-Abri, Abdullah Salim Said Al-Afari, Khalid Sarhan Hamed Al-Hinai, Ammar Khalifa Juma Thunei Maamari, Sulaiman Mohammed Al-Maqrashi, Saif Sultan Al-Mahrouqi, Faisal Abdullah Haji Al-Rahbi, Hussain Said Saad Al-Riyami, Yagdhan Hamood Al-Shuraiqi, Yousuf Abdallah Al-Tobi, Ali Rashid Said and also thank Fakhra Al-Yahmadi and Raya Al-Yahyai for their evaluation of GIS data on radiation levels in Omani oil wells.

References

Abu-Hilal, A.H., 1994. Effect of depositional environment and sources of pollution on uranium concentration in sediment, coral, algae and seagrass species from the Gulf of Aqaba (Red Sea). Mar. Pollut. Bull. 28, 81–88.
Achal, V., Pan, X.L., Zhang, D.Y., 2012. Bioremediation of strontium (Sr) contaminated aquifer quartz sand based on carbonate precipitation induced by Sr resistant *Halomonas* sp. Chemosphere 89, 764–768.
Ahmed, A., Young, S.D., Shaw, G., 2014. Factors affecting uranium and thorium fractionation and profile distribution in contrasting arable and woodland soils. J. Geochem. Explor. 145, 98–105.
Akhtar, K., Akhtar, M.W., Khalid, A.M., 2007. Removal and recovery of uranium from aqueous solutions by *Trichoderma harzianu*. Water Res. 41, 1366–1378.
Al-Balushi, S., 2015. Geochemical Exploration and Mapping of Uranium Deposits in Western Side of Dhofar and the Influence of Regional and Local Geology on the Type and Distribution of Ore Deposits, Earth Science. Sultan Qaboos University, Muscat pp. 78.
Allen, P.A., 2007. The Huqf Supergroup of Oman: basin development and context for Neoproterozoic glaciation. Earth Sci. Rev. 84, 139–185.
Bargar, J.R., Fuller, C.C., Marcus, M.A., Brearley, A.J., De la Rosa, M.P., Webb, S.M., Caldwell, W.A., 2009. Structural characterization of terrestrial microbial Mn oxides from Pinal Creek, AZ. Geochim. Cosmochim. Acta 73, 889–910.
Basu, A., Sanford, R.A., Johnson, T.M., Lundstrom, C.C., Löffler, F.E., 2014. Uranium isotopic fractionation factors during U(VI) reduction by bacterial isolates. Geochim. Cosmochim. Acta 136, 100–113.
Beazley, M.J., Martinez, R.J., Sobecky, P.A., Webb, S.M., Taillefert, M., 2007. Uranium biomineralization as a result of bacterial phosphatase activity: insights from bacterial isolates from a contaminated subsurface. Environ. Sci. Technol. 41, 5701–5707.
Béchennec, F., Le Métour, J., Platel, J.P., Roger, J., 1993. Geological Map of the Sultanate of Oman (1:250000, GIS Version), Explanatory Notes. Ministry of Petroleum and Minerals, Directorate General of Minerals, Sultanate of Oman, Muscat.
Bender, J., Phillips, P., 2004. Microbial mats for multiple applications in aquaculture and bioremediation. Bioresour. Technol. 94, 229–238.
Benzerara, K., Miot, J., Morin, G., Ona-Nguema, G., Skouri-Panet, F., Férard, C., 2011. Significance, mechanisms and environmental implications of microbial biomineralization. Comptes Rendus Geosci. 343, 160–167.
Bethke, C.M., 2008. Geochemical and Biogeochemical Reaction Modeling, 2nd edition. Cambridge University Press pp. 543.
Blancoa, P., Tomé, F.V., Lozano, J.C., 2005. Fractionation of natural radionuclides in soils from a uranium mineralized area in the south-west of Spain. J. Environ. Radioact. 79, 315–330.
BRGM, 1984. Geological Study of the Mineral Occurrence of the Central Part of the Northern Oman mountains. BRGM, Oman p. 289.
Brookins, D.G., 1983. Eh-pH diagrams for the rare earth elements at 25 °C and one bar pressure. Geochem. J. 17, 223–229.
Condomines, M., Morand, P., Allegre, C.J., 1981. ^{230}Th-^{238}U radioactive disequilibria in tholeiites from the FAMOUS zone (MidAtlantic Ridge 36°50'N): Th and Sr isotopic geochemistry. Earth Planet. Sci. Lett. 55, 247–256.
Condomines, M., Bouchez, R., Ma, J.L., Tanguy, J.C., Amosse, J., Piboule, M., 1987. Short-lived radioactive disequilibria and magma dynamics in Etna volcano. Nature 325, 607–609.
Dabous, A.A., Osmond, J.K., Dawood, Y.H., 2002. Uranium/thorium isotope evidence for ground-water history in the Eastern Desert of Egypt. J. Arid Environ. 50, 343–357.
Elliott, T., 1997. Fractionation of U and Th during mantle melting: a reprise. Chem. Geol. 139, 165–183.
Evans, M.A., 1993. Ore Geology and Industrial Minerals—An Introduction. Blackwell Science Ltd.
Forbes, G.A., Jansen, H.S.M., Schreurs, J., 2010. Lexicon of Oman— subsurface stratigraphy. GeoArabia Spec. Publ. 5, 1–371.
Francis, C.A., Tebo, B.M., 2002. Enzymatic manganese(II) oxidation by metabolically dormant spores of diverse Bacillus species. Appl. Environ. Microbiol. 68, 874–880.
Gabelman, J.W., 1988. Classification of uranium deposits. Ore Geol. Rev. 3, 13–29.
Gabelman, J.W., Boyer, W.H., 1988. Uranium deposits in Todilto limestone, New Mexico: the Barbasra "J" No. 1 mine. Ore Geol. Rev. 3, 241–276.
Goldberg, K., Humayun, M., 2016. Geochemical paleoredox indicators in organic-rich

shales of the Irati Formation, Permian of the Paraná Basin, southern Brazil. Braz. J. Geol. 46, 377–393.
Goulhen, F., Gloter, A., Guyot, F., Bruschi, M., 2006. Cr(VI) detoxification by *Desulfovibrio vulgaris* strain *Hildenborough*: microbe-metal interactions studies. Appl. Microbiol. Biotechnol. 71, 892–897.
Grenthe, I., Fuger, J., Konings, R.J.M., Lemire, R.J., Muller, A.B., Nguyen-Trung, C., Wanner, H., 1992. Chemical Thermodynamics: Chemical Thermodynamics of Uranium. OECE-NEA Elsevier pp. 715.
Hersi, S.H., Al-Harthy, A., Abbasi, I.A., Al-Sayigh, A., Al-Lazki, A., 2012. Mesozoic Sedimentary Succession of Jeza-Qamar (Dhofar) Basin: Implications for Exploration Potential of an Overlooked Hydrocarbon System. Unpublished Research Report. Sultan Qaboos University, Oman pp. 160.
Hohmann, C., Winkler, E., Morin, G., Kappler, A., 2010. Anaerobic Fe(II)-oxidizing bacteria show as resistance and immobilize As during Fe(III) mineral precipitation. Environ. Sci. Technol. 44, 94–101.
Howari, F., Goodell, P., Salman, A., 2016. Metallogenic evolution of uranium deposits in the Middle East and North Africa deposits. J. Afr. Earth Sci. 114, 30–42.
IAEA, 1984. Surficial Uranium Deposits. IAEA, Vienna, Austria p. 252.
IAEA, 1985. Geological Environments of Sandstone-Type Uranium Deposits, TECDOC-328. IAEA, Vienna, Austria p. 408.
IAEA, 1986. Vein Type Uranium Deposits. IAEA, Vienna, Austria p. 423.
IAEA, 1987. Uranium Deposits in Proterozoic Quartz-Pebble Conglomerates. IAEA, Vienna, Austria p. 459.
IAEA, 1988. INTURGEO: The International Uranium Geology Information System – A World Atlas of Uranium Occurrences and Deposits. IAEA, Vienna, Austria p. 493.
IAEA, 2009. World Distribution of Uranium Deposits (UDEPO) With Uranium Deposit Classification. IAEA, Vienna, Austria p. 127.
Jroundi, F., Merroun, M.L., Arias, J.M., Rossberg, A., Selenska-Pobell, S., Gonzalez-Munoz, M.T., 2007. Spectroscopic and microscopic characterization of uranium biomineralization in *Myxococcus xanthus*. Geomicrobiol. J. 24, 441–449.
Keppler, H., Wyllie, P.J., 1990. Role of fluids in transport and fractionation of uranium and thorium in magmatic processes. Nature 348, 531–533.
Khoury, H.N., Salameh, E.M., Clark, I.D., 2014. Mineralogy and origin of surficial uranium deposits hosted in travertine and calcrete from central Jordan. Appl. Geochem. 43, 49–65.
Krishnaswami, S., Turekian, K.K., Bennett, J.T., 1984. The behavior of ^{232}Th and the ^{238}U decay chain nuclides during magma formation and volcanism. Geochim. Cosmochim. Acta 48, 505–512.
Landwehr, D., Blundy, J., Chamorro-Perez, M., Hill, E., Wood, B., 2001. U-series disequilibria generated by partial melting of spinel lherzolite. Earth Planet. Sci. Lett. 188, 329–348.
Langmuir, D., 1978. Uranium solution-mineral equilibria at low temperatures with applications to sedimentary ore deposits. Geochim. Cosmochim. Acta 42, 547–569.
Langmuir, D., 1997. Aqueous Environmental Geochemistry. Prentice-Hall, Engelwood Cliffs New Jersey.
LaTourrette, T.Z., Kennedy, A.K., Wasserburg, G.J., 1993. Thorium-uranium fractionation by garnet: evidence for a deep source and rapid rise of oceanic basalts. Science 261, 5122.
Leventhal, J.S., 1991. Comparison of organic geochemistry and metal enrichment in two black shales: Cambrian Alum Shale of Sweden and Devonian Chattanooga Shale of United States. Mineral. Deposita 26, 104–112.
Macaskie, L.E., Empson, R.M., Cheetham, A.K., Grey, C.P., Skarnulis, A.J., 1992. Uranium bioaccumulation by a *Citrobacter sp*. as a result of enzymatically mediated growth of polycrystalline HUO2PO4. Science 257, 782–784.
Marmont, S., 1989. Unconformity-type uranium deposits. In: Roberts, R.G., Sheahan, P.A. (Eds.), Ore Deposit Models. Geological Association of Canada, Newfoundland, pp. 103–115.
Mercolli, I., Briner, A.P., Frei, R., Schonberg, R., Nagler, T.F., Kramers, J., Peters, T., 2006. Lithostratigraphy and geochronology of the Neoproterozoic crystalline basement of Salalah, Dhofar, Sultanate of Oman. Precambrian Res. 145 (3), 182–206.
Min, M., Peng, X., Wang, J., Osmond, J.K., 2005. Uranium-series disequilibria as a means to study recent migration of uranium in a sandstone-hosted uranium deposit, NW China. Appl. Radiat. Isot. 63, 115–125.
Miot, J., Benzerara, K., Morin, G., Kappler, A., Bernard, S., Obst, M., Férard, C., Skouri-Panet, F., Guigner, J.M., Posth, N., Galvez, M., Brown Jr, G.E., Guyot, F., 2009. Iron biomineralization by neutrophilic iron-oxidizing bacteria. Geochim. Cosmochim. Acta 73, 696–711.
Misaelides, P., Godelitsas, A., Filippidis, A., Charistos, D., Anousi, I., 1995. Thorium and uranium uptake by natural zeolitic materials. Sci. Total Environ. 173/174, 237–246.
Newman, S., Finkel, R.C., Macdougall, J.D., 1984. Comparison of ^{230}Th-^{238}U disequilibrium systematics in lavas from three hot spot regions: Hawaii, Prince Edward and Samoa. Geochim. Cosmochim. Acta 48, 315–324.
Nishimura, S., 1970. Disequilibrium of the ^{238}U series in recent volcanic rocks. Earth Planet. Sci. Lett. 293–300.
Noller, B.N., Watters, R.A., Woods, P.H., 1997. The role of biogeochemical processes in minimising uranium dispersion from a mine site. J. Geochem. Explor. 58, 37–50.
Ohkouchi, N., Kuroda, J., Taira, A., 2015. The origin of Cretaceous black shales: a change in the surface ocean ecosystem and its triggers. Proc. Jpn. Acad. Ser. B: Phys. Biol. Sci. 91, 273–291.
Oversby, V.M., Gast, P.W., 1968. Lead isotope compositions and uranium decay series disequilibrium in recent volcanic rocks. Earth Planet. Sci. Lett. 5, 199–206.
Pan, X.L., Wang, J.L., Zhang, D.Y., 2009. Biosorption of strontium ion by immobilized *Aspergillus niger*. Int. J. Environ. Pollut. 37, 276–288.
Pracejus, B., 2015. The Ore Minerals Under the Microscope – An Optical Guide, 2nd ed. Elsevier, Amsterdam.
Quidwai, H.A., 1981. Wadi Gharbatan Uranium Prospect – Final Report. Ministry of Petroleum and Minerals, Oman.
Quidwai, H.A., Khalifa, M.I., 1982. Ground Follow-Up of the Airborne Radiometric Anomalies in South Western Dhofar, Sultanate of Oman. Ministry of Petroleum and Minerals.
Ragland, P.C., Billings, G.K., Adams, J.A.S., 1967. Chemical fractionation and its relationship to the distribution of thorium and uranium in a zoned granite batholith. Geochim. Cosmochim. Acta 31, 17–33.
Russel, A.D., Emerson, S., Nelson, B.K., Erez, J., Lea, D.W., 1994. Uranium in foraminiferal calcite as a recorder of seawater uranium concentrations. Geochim. Cosmochim. Acta 58, 671–681.
Schmidt, M., Lee, S.S., Wilson, R.E., Soderholm, L., Fenter, P., 2012. Sorption of tetravalent thorium on muscovite. Geochim. Cosmochim. Acta 88, 66–76.
Spiegelman, M., Elliott, T., 1993. Consequences of melt transport for uranium series disequilibrium. Earth Planet. Sci. Lett. 118, 1–20.
Spiro, T.G., Bargar, J.R., Sposito, G., Tebo, B.M., 2010. Bacteriogenic manganese oxides. Acc. Chem. Res. 43, 2–9.
Sundararajan, N., Pracejus, B., Al-Khirbash, S., Al-Lazki, A., Al-Hosni, T., Al-Mushani, M., 2013. Uranium and Associated Minerals in the Sultanate of Oman – Geophysical and Geochemical Exploration, First Annual Report. Ministry of Commerce & Industry, Oman, Muscat pp. 5.
Sundararajan, N., Pracejus, B., Al-Khirbash, S., Al-Lazki, A., Al-Hosni, T., Al-Mushani, M., 2014. Uranium and Associated Minerals in the Sultanate of Oman – Geophysical and Geochemical Exploration, Second Annual Report. Ministry of Commerce & Industry, Oman pp. 31.
Sundararajan, N., Pracejus, B., Al-Khirbash, S., Al-Hosni, T.K., Ebrahimi, A., Al-Mushani, M., Al-Aamr, Z., 2015a. Goa, IndiaVery Low Frequency Electromagnetic (VLF-EM) Investigation for Uranium in Dhofar Region, Sultanate of Oman, Indian Geophysical Union: 52nd Annual Convention on “Near Surface Earth System Science”2015. Very Low Frequency Electromagnetic (VLF-EM) Investigation for Uranium in Dhofar Region, Sultanate of Oman, Indian Geophysical Union: 52nd Annual Convention on “Near Surface Earth System Science”.
Sundararajan, N., Pracejus, B., Al-Khirbash, S., Al-Lazki, A., Al-Hosni, T., Al-Mushani, M., 2015b. Uranium and Associated Minerals in the Sultanate of Oman – Geophysical and Geochemical Exploration, Third Annual Report. Ministry of Commerce & Industry, Oman, Muscat pp. 38.
Sundararajan, N., Pracejus, B., Al-Khirbash, S., Al-Hosni, T., Ebrahimy, A., Al-Maashani, M., 2016. Magnetic mapping of structures favorable to uranium mineralization. Dhofar Region, Sultanate of Oman, 13th Annual Meeting of Asia Oceania Geosciences Society at China (AOGS).
Sundararajan, N., Pracejus, B., Al-Khirbash, S., Al-Hosni, T., Ebrahimi, A., Al-Mushani, M., 2017. Magnetic mapping for delineating structures favorable to uranium mineralization in Dhofar Region, Sultanate of Oman. Int. J. Earth Environ. Sci. 2, 1–9.
Tebo, B.M., Johnson, H.A., McCarthy, J.K., Templeton, A.S., 2005. Geomicrobiology of manganese(II) oxidation. Trends Microbiol. 13, 421–428.
Templeton, A.S., Trainor, T.P., Traina, S.J., Spormann, A.M., Brown Jr, G.E., 2001. Pb(II) distributions at biofilm-metal oxide interfaces. Proc. Natl. Acad. Sci. U. S. A. 98, 11897–11902.
Thompson, G., Livingston, H.D., 1970. Strontium and uranium concentration in aragonite precipitated by some modern corals. Earth Planet. Sci. Lett. 8, 439–442.
Valsami-Jones, E., Ragnarsdóttir, K.V., 1997. Controls on uranium and thorium behaviour in ocean-floor hydrothermal systems: examples from the Pindos ophiolite, Greece. Chem. Geol. 135, 263–274.
Vargas, M.J., Tomé, F.V., Sánchez, A.M., Vásquez, M.T.C., Murillo, J.L.G., 1997. Distribution of uranium and thorium in sediments and plants from a granitic fluvial area. Int. J. Appl. Radiat. Isot. 48, 1137–1143.
Warren, L.A., Haack, E.A., 2001. Biogeochemical controls on metal behaviour in freshwater environments. Earth Sci. Rev. 54, 261–320.
White, W.M., 2015. Isotope Geochemistry. Wiley-Blackwell.
Wynes, R., Platel, J.P., 1992. Mineralisations uranifères de la Raysut map area (sheet NE 39-16 c- scale 1:100000), recherche d’un eventuel contrôle structural. Sultante of Oman, Minstry of Petroleum and Minerals, directorate General of Minerals.
Zhang, Y., Zhang, Q., Cai, Y., Wang, D., Li, K., 2015. The occurrence state of vanadium in the black shale-hosted vanadium deposits in Shangling of Guangxi Province, China. Chin. J. Geochem. 34, 484–497.